

Contents lists available at ScienceDirect

Geoderma

journal homepage: www.elsevier.com/locate/geoderma





Trace metals and metalloids and Ga/Al ratios in grey shale weathering profiles along a climate gradient and in batch reactors

Justin B. Richardson a,b,*, Ivan C. Mischenko Trevor J. Mackowiak c, Nicolas Perdrial C

- ^a Department of Geoscience, University of Massachusetts Amherst, Amherst, MA 01003, USA
- ^b School of Earth and Sustainability, University of Massachusetts Amherst, Amherst, MA 01003, USA
- ^c Department of Geology, University of Vermont, 180 Colchester Avenue, Burlington, VT 05405, USA

ARTICLE INFO

Handling Editor: Daniel Said-Pullicino

Keywords:
Potentially toxic elements
Toxic metals
Regolith
Critical Zone
Alfisols
Ultisols

ABSTRACT

Shale is an important lithology globally due to its wide spatial abundance and potentially high trace metal and metalloid (TMM) geochemistry, which can be potentially inherited by its overlying soils. Unlike other soils, shale-derived soils inherit organic matter and oxides (Fe and Mn) which promote accumulation and retention of both geogenic and exogeneous TMMs. Here, we explore TMMs in seven grey shales weathering profiles along a north-south transect spanning the western flank of the Appalachian Mountains from New York to Tennessee. Overall, total TMM concentrations in the grey shales and their soils were below concentrations known to be toxic and below concentrations observed in black shales. Tau values show that shale-derived soils are net accumulators of many TMMs (As, Cd, Co, Cu, Ni, Pb, Sb, Sn and Zn) but others (Cr, W, and V) showed a net depletion. Many of the TMMs had high proportions (5-50%) that were sequestered in reducible phases (amorphous and crystalline Fe oxides) but few TMMs were associated with oxidizable phases (organic matter, reduced minerals). Sulfides and oxides (Mn nor Fe) were not detected by X-ray diffraction (<2% g/g). TMM accumulation and release during weathering was not extensively related to climate or soil development/age as we hypothesized, potentially due to localized effects of vegetation, geomorphology, pollution, and physicochemical parameters of the shale. Our laboratory batch reactor experiments indicated that some TMMs had highest release rates under oxic, acidic conditions with organic acids present (Cr., Ga., Sn., Sb., and W) implying aluminosilicate dissolution control or under slightly acidic, reduced conditions (As, Cd, Co, Cu, Ni, Pb, V, and Zn), suggesting association with geogenic oxides. Total Ga/Al ratios in rock to soil profiles were not varying significantly across the climate-soil development gradient, despite batch reactor acidic conditions generating low Ga/Al ratios. This implies weathering of shales is dominated by processes that do not fractionate Ga/Al ratio (organic or inorganic colloid production) as our laboratory results suggests oxic, acidic aluminosilicate weathering should generate a high Ga/Al solid phase.

1. Introduction

Shale is an important lithology both globally and for the United States due to its wide spatial abundance and its geochemistry (United States Energy Information Administration and Kuuskraa, 2011). Shales, both grey and black varieties, can have higher trace metal and metalloid (TMMs) concentrations than igneous or metamorphic rocks due to their sedimentary origin and high organic content (Vine and Tourtelot, 1970; Perkins and Mason, 2015) For example, Perkins and Mason (2015) observed concentrations of As, Cd, Cu, Mo, Ni, V and Zn five times higher than typical crustal abundance in black shales and further noted their ability to generate hazardous concentrations of As, Cd, Co, Pb in

water extractions. High TMM concentrations in shales and other sedimentary rocks can be inherited by the overlying soils. Further, Liu et al., (2017) observed that agricultural soils derived from black shales globally tend to have Cd concentrations that posed a potential hazard to human health, especially to food crops like rice. Similarly, argillite at the Eel River CZO generated high Hg soil concentrations (Richardson et al., 2018). However, pollutant TMMs like Cd and Pb can be sequestered in shale-derived soils (e.g. Ma et al., 2014; Liu et al., 2017) due to their high surface area from clay-sized fraction, diagenetic phyllosilicates, inherited geogenic and added organic matter, and inherited geogenic Fe oxides and sulfides (Hosterman and Whitlow, 1981; Fu et al., 2015). Thus, soils derived from shale have the potential to sequester TMMs

^{*} Corresponding author at: University of Massachusetts Amherst, 233 Morrill Science Center, Amherst MA 01003, USA. *E-mail address:* jbrichardson@umass.edu (J.B. Richardson).

from smelting, automobile exhaust, coal combustion, and other forms of local and regional anthropogenic atmospheric pollution (Lyons et al., 2006; Herndon and Brantley, 2011; Ma et al., 2014).

The transport and sequestration of TMMs in soils is dependent on the formation of Fe and Mn oxyhydroxides and accumulation of new organic matter from plant detritus (Dere et al., 2016), which is dependent on the extent of pedogenesis. An important difference between shale and other sedimentary rock derived soils and more crystalline igneous and metamorphic rocks derived soils is the inheritance of many of these properties. For example, shale soil percent Loss On Ignition (%LOI) were commonly > 4% throughout entire weathering profiles across climates (Dere et al., 2013) while total organic carbon decreased to < 0.5 %below 1 m depth in igneous and metamorphic profiles (Richardson et al., 2018). Further, Perkins and Mason (2015) and Fu et al., (2015) found evidence that metals can be inherited from reduced (pyrite) and oxidized (hematite) present in shales. These TMM bearing Fe minerals can be inherited by soils forming from shale, as Fe and associated TMMs are recalcitrant during pedogenesis (Hieronymus et al., 2001; Yesavage et al., 2012). Thus, highly developed soils such as Ultisols may not contain high TMMs due to extensive weathering and loss of geogenic TMM bearing minerals. Conversely, very young soils, such as inceptisols in recently glaciated areas may still possess high TMM bearing minerals.

Here, we are concerned with grey shales derived soils along a north-south transect along the western flank of the Appalachian mountains as a proxy to explore pedogenesis, manifested through both soil age and climate. The shale derived soils of New York, northern Pennsylvania, and northern Ohio are < 14,000 yr in age due to the Wisconsin glaciation and periglacial/glacial conditions (Ciolkosz et al., 1989; Ciolkosz et al., 1990). These soils are typically young Inceptisols or Alfisols and exhibit high base cation saturation and can accumulate organic matter in their epipedons due the recent glaciation and shorter, cooler summers. Further south, shale-derived soils of Kentucky and Tennessee on stable landforms are much older Ultisols in a warmer and slightly wetter climate (National Oceanographic and Atmospheric Administration (NOAA), 2011). These differences in pedogenic development can influence the retention of TMMs in the soil profile from loss or neoformation of organic matter or secondary oxides. A similar transect was explored by Dere et al. (2013) for macro elements (Si, Al, Na, K, Fe) and by Jin et al. (2017) for rare earth elements (REEs) showing that pedogenesis had substantially affected the physiochemical nature of the soils derived from shales. However, the mechanisms of inheritance and dissolution as well as human additions to elements, particularly TMMs remain understudied and poorly constrained.

It is essential to utilize established and novel geochemical tools to determine geogenic sourcing of elements and weathering pathways. One important method is normalization to refractory indexing elements, such as Ti and Zr, to calculate tau (τ) values to distinguish between added TMMs from the atmospheric and biological cycling from inherited TMM from shale weathering. Estimating sequestered TMMs from the atmosphere and biological cycling and inherited TMM from shale is key for determining if the shale-derived soils are a net sink or source for potential TMM pollution to groundwater resources and surface water ecosystems. Furthermore, weathering pathways may be explored using comparisons among TMMs. Here, we seek to employ Ga/Al ratios to determine if aluminosilicate weathering is congruent, resulting in dissolution and loss of TMMs or incongruent, resulting in neoformed clays and oxide minerals which can sequester additional TMMs. Ga/Al ratios across lithologies is nearly consistent, ranging between 0.07 and 0.12 mmol/mol across United States Geological Survey (USGS) rock standards: BHVO-2 basalt, RGM rhyolite, W-2 diabase, SBC-1 shale. In particular, if Ga is sequestered in secondary oxides and Al is lost, we would expect an increase in the Ga/Al ratio (Hieronymus et al., 2001) but if Ga is more mobile than Al during silicate dissolution, Ga/Al ratios decrease (Shiller and Frilot, 1996). Thus, tau normalization to Ti and application of Ga/Al ratios can shed insight on total losses and potentially the type mechanism of shale dissolution and weathering.

The objectives of this study were to (1) quantify the accumulation and release of TMMs from shales, (2) explore the mechanism of TMM retention by characterizing their distribution in organic and oxide phases, particularly with tau values and Ga/Al ratios, (3) determine the effect of pedogenesis via climate (mean annual precipitation and mean annual temperature) and soil age, and lastly (4) evaluate how solution chemistry can affect TMM release. Shale can have higher TMM concentrations than other rock types and thus can be an important source to surface waters, ground waters and their derived soils. However, high surface area and inherited clay content, organic matter, and oxides (Fe) present in shale can act as a sink for TMMs derived from the atmosphere or retained during weathering. Further, the type of weathering can affect the rate at which TMMs are mobilized from solid phase to aqueous phases and may be elucidated through specific phase extractions, tau values, and application of Ga/Al ratios. Lastly, climate can affect these processes as greater temperatures can decrease organic matter stabilization but may increase Fe oxide formation. Exploring the retention or release of TMMs from shale can highlight the importance of shalederived soils in the terrestrial TMM biogeochemical cycling as sources

2. Materials and methods

2.1. Site descriptions and soil and rock sampling

Seven sites with similar grey shale lithology and mixed northern forests were chosen, spanning central New York to eastern Tennessee (Fig. 1), nearly 7° latitude difference with 6.3° C change in Mean Annual Temperature (MAT) (Table 1). Lithology was evaluated using digital USGS maps and tools to identify shale formations and groups (https://mrdata.usgs.gov/geology/state/). Satellite orthoimagery, USGS state geologic maps, and Google© street view was used to identify outcrops and road cuts to sample. Lithology at each site was confirmed with hand samples from outcrops. Low organic, grey shales were studied to avoid their wide variation in TMM chemistry. Vegetation across sites were northern hardwoods transitioning into mixed hardwoods; the most dominant species were *Quercus* spp., *Carya* spp., *Acer* spp., *Fagus grandifolia*, *Juglans* spp., and *Populus* spp. with interspersed conifers, dominated by *Pinus* spp., and *Tsuga canadensis*.

At each site, a soil profile with exposed bedrock on shoulder slopes of hills and plateaus were identified. Soil pit locations were rejected if evidence of erosion, sediment deposition, and microtopographical lows were present. At each site, one soil pit was excavated using stainless-steel tile spades and pry bars until refusal. The lower boundary of the soil pits were characterized by 50–150 mm chips of shale. One sample was collected for each 5 cm depth increment from the soil surface to the lower boundary of excavation. Three samples of unweathered shale and partially-weathered were collected from either the road cut exposure or natural outcrop. Soils and weathered bedrock samples were dried in a convection oven at 70 °C for 72 h. After drying, soils were sieved to $<2\,$ mm, often using a stainless-steel hammer to disaggregate the clay-rich soil peds of the Bt horizons. Weathered and unweathered shale rock samples were ground with a tungstate mill and passed through a 100-mesh sieve ($<150\,\mu m$).

2.2. Soil and rock physicochemical analyses

Soil pH was determined using a 2:5 soil—water slurry method. In brief, 4 g of soil and 10 g of 0.1 M $CaCl_2$ were shaken, settled overnight and the pH of the supernatant extract was measured with a VWR 8051 pH meter. Loss-on-ignition was used to estimate % soil organic matter (SOM) and measured by combusting a 5 g oven-dried subsample at 550 °C for 8 hrs. Every 20 samples included one blank and duplicate. Samples were analysed for soil particle size distribution using sedimentation columns and Bouyoucos hydrometer method (Gee et al., 1986). For each analysis, \sim 30 g of dried soil was weighed into 250 mL

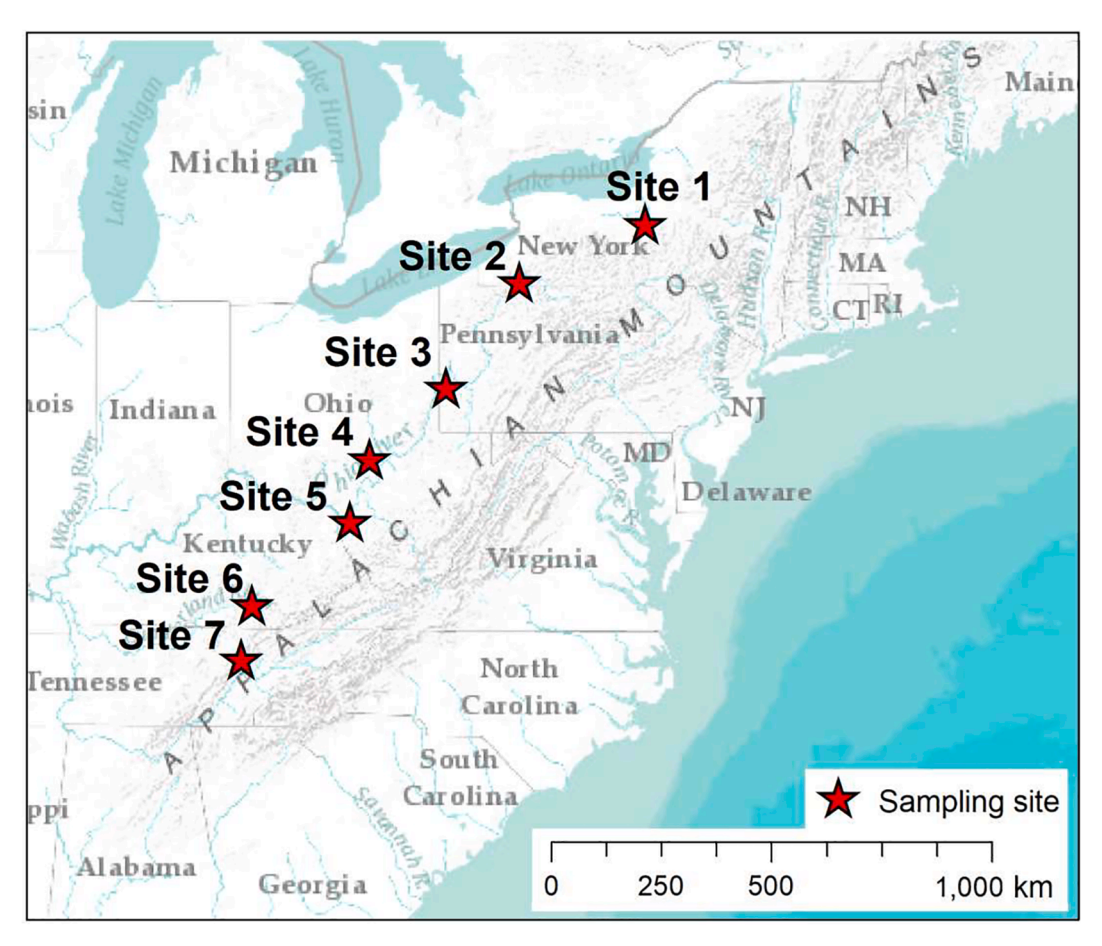


Fig. 1. Map of sampling site locations in this study.

Table 1
Site locations, lithology, and soil taxonomy and geomorphic setting.

Site #	Longitude	Latitude	MAT† °C/ yr	MAP† mm/ yr	Soil Series‡	Great Group‡	Age/Rock§	Landform‡
Site 1	-76.3257	42.9082	8.6	1067	Schoharie silty clay	Hapludalfs	Middle Devonian Shale	Hill and hillslope
Site 2	-78.8892	42.0367	7.3	1135	Rayne silt loam	Hapludults	Upper Devonian Shale	Hills, Plateaus
Site 3	-80.3866	40.4205	11.1	960	Dormont silt loam	Hapludalfs	Pennsylvanian Shale	Hill and hillslope
Site 4	-81.9385	39.3031	11.0	1001	Westmoreland silt loam	Ultic Hapludalfs	Pennsylvanian Shale, Siltstone, Mudstone	Hill and hillslope
Site 5	-82.3485	38.3037	12.3	1138	Gilpin-Upshur silt loam	Hapludults	Pennsylvanian Shale, Siltstone, Mudstone	Ridge, hill, and hillslope
Site 6	-84.3458	36.9565	13.2	1255	Shelocta-Rigley-Latham- Lily	Hapludults	Pennsylvanian Shale, Siltstone	upland areas, foot slopes
Site 7	-84.5521	36.0722	14.9	1293	Lonewood silt loam	Hapludults	Pennsylvanian Shale, Sandstone	Rolling plateaus

†Mean annual temperature (MAT) and mean annual precipitation (MAP) for 30-year averages for 1980 to 2010 was obtained from the nearest weather station for each site (National Oceanographic and Atmospheric Administration (NOAA), 2011).

‡Soil series information was obtained from the USDA NRCS Web Soil Survey and field measurements. (https://websoilsurvey.sc.egov.usda.gov/App/WebSoilSurvey.aspx accessed 16 Aug 2020).

§Geologic information was from USGS (https://mrdata.usgs.gov/geology/state/).

glass beaker. Organic matter was removed and 100 mL of 1 M sodium hexametaphosphate (HMP)was added to the soil solution which sat for at least 8 h to disperse soil particles. This HMP-soil slurry was washed out into a 1000 mL graduated cylinder with DI water. A modified Bouyoucos hydrometer method was used, with hydrometer readings at 60 s and 1.5 hr after mixing to the closest 0.5 g $\rm L^{-1}$.

2.3. Soil and rock extractions and digestions for TMMs

A sequential extraction was performed for insight to the phase

partitioning of TMMs in soils and bedrock. The first extraction was to oxidize organic matter. First, a 1 g sample of soil or bedrock was extracted by slowly adding 20 mL of 15% $\rm H_2O_2$ solution over 4 h and then shaking for 20 h. The slurry was centrifuged at 3000 rpm for 1 hr and the supernatant was transferred to a 50 mL centrifuge tube. The remaining extractant was reduced to extract secondary oxide phases using a modified citrate-bicarbonate-dithionite (CBD) extraction (Raiswell et al., 1994; Mehra and Jackson, 2013). In brief, 0.5 g of sodium dithionite were added to the remaining soil mass. Then 40 mL of 0.1 M sodium citrate buffered with 0.1 M sodium bicarbonate solution was

added to each tube and sealed tightly. The extracts were then heated to 60 $^{\circ}\text{C}$ in a convection oven for 12 h. For elemental analysis, both the oxidizable and reducible fractions were diluted with 5 g oxidizable extract diluted with 5 g of 2.5% HNO_3 solution and 0.2 g of the reducible fraction diluted with 14.8 g of 2.5% HNO_3 solution. Since the reducible fraction was under basic conditions at pH 8.1 and utilized high sodium concentrations, it was imperative to use a small amount to keep metals and citrate in solution while acidifying. With every 20 samples, a preparation blank, a duplicate, and a NIST San Joaquin 2709a was included.

Total digestion was conducted using a 50 mg subsample digestion that was placed in a 15 mL PFLA vial with 2.5 mL of 25 M HF acid and 2.5 mL of distilled 16 M HNO $_3$ (Trace metal grade, VWR Analytical, Radnor, PA, USA), sealed with a lid and heated to 150 °C. After complete digestion of most visible materials, samples were dried to volatize Si-F complexes and redissolved in 5 mL of 8 M HNO $_3$ and re-sealed and heated to 150 °C. The final digestate was diluted to 50 mL using 18.2 M $_2$ 0 deionized water. With every 20 samples, at least one preparation blank, one duplicate, and a standard reference material (SRM) USGS SBC-1 was included. TMM concentrations data are available in the Supplemental Information.

2.4. Batch reactors

Batch reactors were conducted to evaluate the effects of organic acids, reducing conditions, and pH on TMM release from one shale, from Site 1. In brief, 5.000 g \pm 0.010 g of unweathered shale (URW) from each site was weighed into each tube and immersed in 30 mL of treatment solution in acid-washed 50 mL centrifuge tubes. In total, eight treatments were applied with six replicates for 48 batch reactors. Control: native pH and 0.02 M NaCl. Treatment 1: HCl to pH 4.1 and 0.02 M NaCl. Treatment 2: 0.02 M sodium bicarbonate at pH 8.1 and 0.02 M NaCl. Treatments 3 through 5 explored the effects of chelation on shale TMM release with added solution of organics: 0.01 M citric acid and 0.01 M oxalic acid at pH 4.1. Treatment 4: added solution of organics: 0.01 M sodium citrate and 0.01 M sodium oxalate titrated to pH 5.9 with concentrated NaOH. Treatment 5: added solution of organics: 0.01 M sodium citrate and 0.01 M sodium oxalate raised to pH 8.3 with concentrated NaOH and 0.02 M sodium bicarbonate. Treatments 6 and 7 investigated reduced conditions on shale TMM release, using dithionite to turn solutions into strongly reducing conditions. Treatment 6: 0.2 g of sodium dithionite without any organics or buffering agents. Treatment 7: 0.2 g of sodium dithionite with 0.02 M sodium bicarbonate to buffer the solution at pH 8.2. Solutions were shaken with an Eberbach table-top reciprocating shaker at 180 oscillations per minute for 7 d. Samples were then centrifuged at 2500 rpm for 1 hr, supernatant decanted, and filtered $< 0.45 \mu m$. Solution pH of the supernatants was remeasured to determine the change in pH. Batch reactor solutions were acidified to pH 1 with 0.2 g of 15 M HNO₃.

2.5. Elemental analyses

Total digests, oxidizable and reducible extracts, and batch reactor solutions were analyzed for macroelements (Al, Fe, Ca, K, Mg, Mn, and Si except for total digests) using an Agilent 5110 Inductively Coupled Plasma-Optical Emission Spectrometer (Agilent Technologies, Santa Clara, California, USA). Al, Fe, Ca, K, Mg, and Mn concentrations in the preparation blank were <0.05~mg/kg and all duplicates were within 15 % CV. Iron recovery in the total digestions for USGS SBC-1 were >90% of their certified values. Solutions were analyzed for TMMs (As, Cd, Cr, Co, Cu, Ga, Ni, Pb, Sn, Sb, Ti, W, V and Zn) with an Agilent $7700\times$ Inductively Coupled Plasma-Mass Spectrometer. TMMs in the preparation blank were <0.1~ng/g and all duplicates were within 12 % coefficient of variation (CV). Recovery for TMMs in USGS SBC-1 by total digestion was >82% of their certified values. Since oxidizable and reducible fraction are not certified methods, oxidizable and reducible

TMMs cannot be certified for precision and accuracy.

2.6. Mineralogical analyses

Mineralogical characterization of the shale samples was performed by X-ray diffraction on random powder mounts and orientated mounts for in-depth clay mineral identification. For quantification, approximately 0.5 g of each sample was mounted on a glass slide and analyzed between 5 and 55° 20 (0.02° resolution, 1°/min) using a Rigaku Miniflex-2 equipped with a Cu K_{α} X-ray source. Quantification was performed using the Rietveld whole pattern profile fit module in PDXL2 (Rigaku corporation 2007–2017). In depth clay characterization consisted in comparing peak positions and intensities across three dedicated treatments for each sample: air drying, ethylene glycol solvation, 400 °C heat treatment for 35 min (Moore & Reynolds, 1997; Schroeder, 2018) (Supplemental Fig. 1).

2.7. Quantifying tau values and other data analyses

Mass transfer coefficients (τ) of trace metals and metalloids were calculated to measure the degree of depletion or enrichment of regolith, relative to the parent material, for specific elements using Ti as an index element (Brimhall and Dietrich, 1987) and Eq. (1) was derived from Anderson et al., (2002). Mass transfer coefficients are defined for the element of interest (j) in the weathered soil or regolith sample (w) normalized to an immobile index element Ti (i) in the parent material (p).

$$\tau_{j,w} = \frac{C_{j,w}C_{i,p}}{C_{j,p}C_{i,w}} - 1$$

The variables $C_{j,w}$ and $C_{i,w}$ are equal to total concentrations of the element of interest (e.g. TMMs, Fe) and Ti in the weathered samples, respectively, and $C_{j,p}$ and $C_{i,p}$ are the element of interest and Ti concentrations in the parent material (here, the least weathered regolith material) (e.g. Brimhall and Dietrich, 1987; Anderson et al., 2002). Negative τ values indicate a net loss of an element from a specific depth due to leaching. Positive τ values indicate a net enrichment of an element. Unweathered bedrock shale samples in each regolith profile were used as the reference material (e.g. Jin et al., 2017; Richardson et al., 2018). Although Zr and Nb are more immobile (see Kurtz et al., 2000), Ti exists in higher concentrations and avoids errors associated with anomalies in zircon crystal abundance and incomplete zircon digestion.

Linear regression matrix were calculated to determine the association of TMMs with each other, with secondary oxides (Fe reducible fraction), with soil pH, and with percent Loss on Ignition (%LOI) as a proxy for organic matter using Matlab (Matlab 2016, Mathworks, Natick, MA). The regression coefficients and their significance can be found in Supplemental Tables 1–3. In addition, average total soil profile TMMs and soil properties were compared with MAT and Mean Annual Precipitation (MAP) for each site using linear regressions and is available in Supplemental Table 4.

3. Results

3.1. Soil physicochemical properties and macro elements

We characterized soil profile %LOI and pH differences among sites with depth (Fig. 2). Soil pH was highest at Sites 1, 4, and 5 (5.0–6.7) but lower at Sites 2, 6, and 7 (3.1 to 4.7). Overall, %LOI was greatest in surface soils in the 0–15 cm in depths (7%–50% LOI), which coincide with the lowest soil pH values. %LOI was greatest in surface soils at Site 2 followed by Site 7. Soil texture was comparable for all sites: Sites 1, 4, and 5were Loams, Sites 2 and 6 were Silt Loams, Site 7 was a Clay Loam and Site 3 was a Sandy Clay Loam and clay contents ranged from 11 to 35% across the seven sites. MAT and MAP were not correlated with CEC

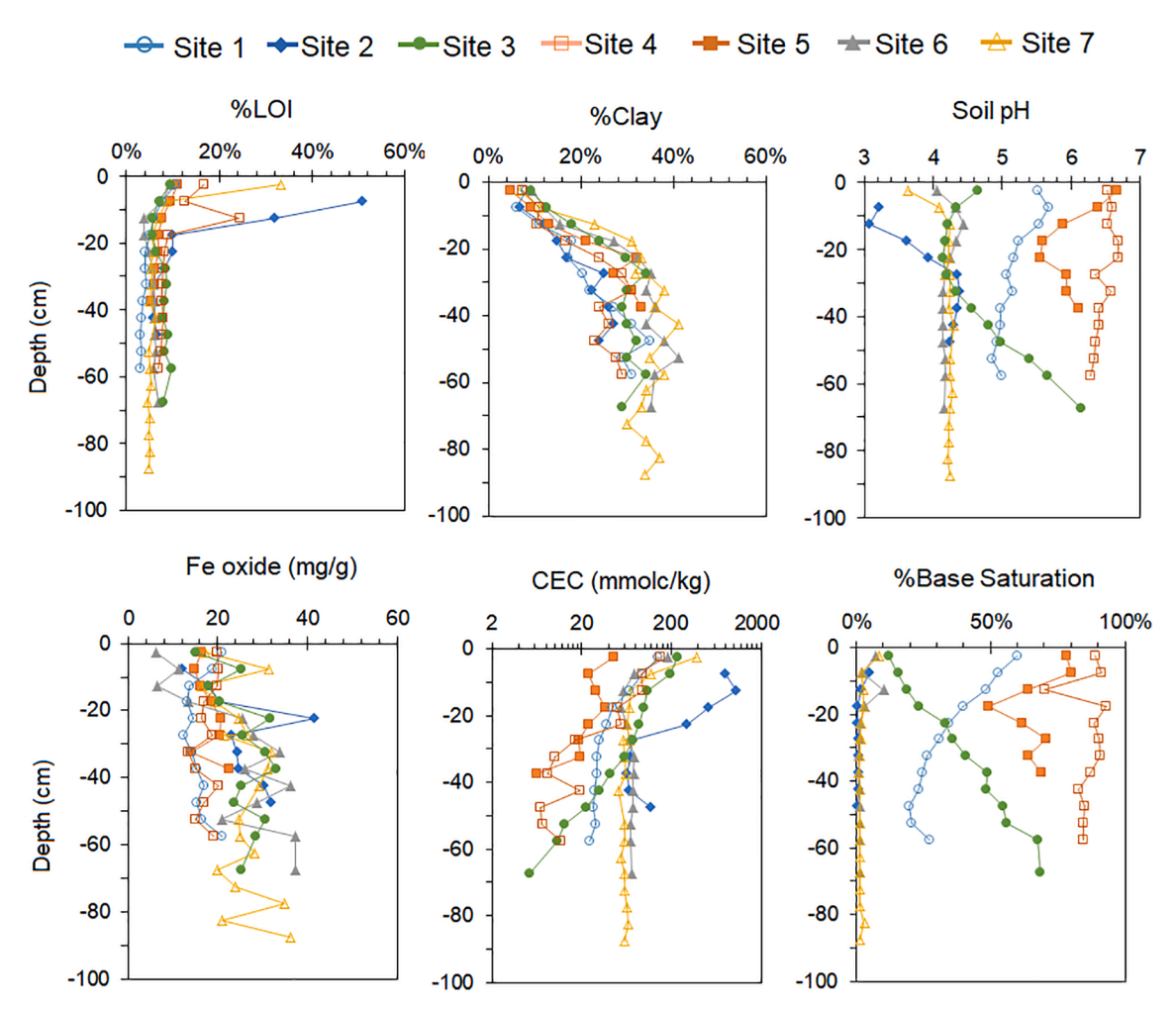


Fig. 2. Soil pH (2:5 soil:water ratio in 0.01 M CaCl₂), %LOI, %Clay, and %Base Saturation profiles for each site. Fe oxide was estimated as the reducible Fe fraction.

(cmol/kg), %base saturation ([Ca, Mg, K, Na]/CEC), or %Clay.

Based upon clay content, base saturation (>35% exchangeable Ca, Mg, K, and Na and low exchangeable Al and Fe, Fig. 2) of surface horizons and subsurface horizons, soils at Sites 1, 3, 4 and 5 classify as Alfisols, which largely agrees with the USDA Web Soil Survey except for Site 5 which was mapped as an Ultisol. Soils at Sites 2, 6, and 7 classify as Ultisols based upon the depletion of exchangeable Ca, Mg, Na, and K and enrichment of exchangeable Al and Fe throughout the weathering profile (see Supplemental data). Macro element concentration and tau profiles of Al, Fe, K, and Na show the extent of pedogenesis of the shalederived soils. Total Al concentrations were largely similar across sites, except for subsurface peaks and depletions at Sites 3 and 6 (Supplemental Fig. 2). Total Fe concentrations with depth were comparable for most sites, except for Site 6 which had subsurface peaks and depletion zones (Supplemental Fig. 2). Total K concentrations were largely similar across sites while total Na had substantial variations: Sites 6 and 7 had the lowest total Na soil concentrations (<1 mg/g) while Sites 1 and 4 had the highest total Na soil concentrations (>3 mg/g).

Tau plots for Al, Fe, K, and Na were calculated to estimate if the elements are depleted or enriched with respect to the shale parent material. Sites 3, 4, and 7 show enrichment in Al while Sites 1, 2, 5, and 6 show some depletion of Al (Supplemental Fig. 2). Nearly all sites exhibit some enrichment of Fe in the soil profile and Sites 1, 3, and 5 show some surficial depletion of Fe (Supplemental Fig. 2). The most southern Sites 4, 5, 6, and 7 show depletion of K and Na for most of the soil profile while the most northern Sites 1, 2, and 3 show limited depletion, especially deeper in the soil profile (>20 cm depth).

3.2. Total TMM concentrations and tau values

For the first hypothesis, TMM profiles for the seven weathering profiles were investigated, to examine their retention or loss from unweathered shale to highly weathered soil horizons (Fig. 3). Arsenic concentrations were within the range of soils globally (0.1-55 mg/kg; Adriano, 2001). However, As concentrations were substantially higher in a subsurface peak at Site 6 at 25 cm depth and As concentrations were greatest in weathered and unweathered shale at Sites 1 and 2. Total Cd, Pb, and Sb concentrations were comparable across sites throughout most of the soil profile, except for high Cd and Sb at Site 1 in the weathered and unweathered bedrock and the surficial peak of Pb at Site 2 (Fig. 3). Total Co, Cr, Cu, Ga, and Ni concentrations were comparable to typical soil concentrations globally (Co = 5-12 mg/kg, Cr = 10-150 mg/kg, Cu = 1-140 mg/kg, Ga = 3-50 mg/kg; Ni = 17-50 mg/kg; Adriano, 2001; Kabata-Pendias and Szteke, 2015). Total W and V concentrations were comparable across sites and near their typical soil concentrations (W = 0.2-5 mg/kg and V = 70-320 mg/kg) (Kabata-Pendias and Szteke, 2015), except for high rock W concentrations at Site 2 and high rock V concentrations at Site 1 (Fig. 3). Total Sn and Zn concentrations exhibited a high variation within soil profiles and among sites. Total Sn concentrations at Sites 1, 3, 5, and 6 ranged within typical concentrations of 0.1-10 mg/kg but total Sn concentrations were elevated at Sites 2, 4, and 7 (Kabata-Pendias and Szteke, 2015). Total Zn concentrations were at the high end of typical soil concentrations of 10-300 mg/kg (Adriano, 2001), with high Zn concentration peaks in the soil profile at Sites 2 and 6 (Fig. 3).

The relationships among total TMM concentrations and with climate

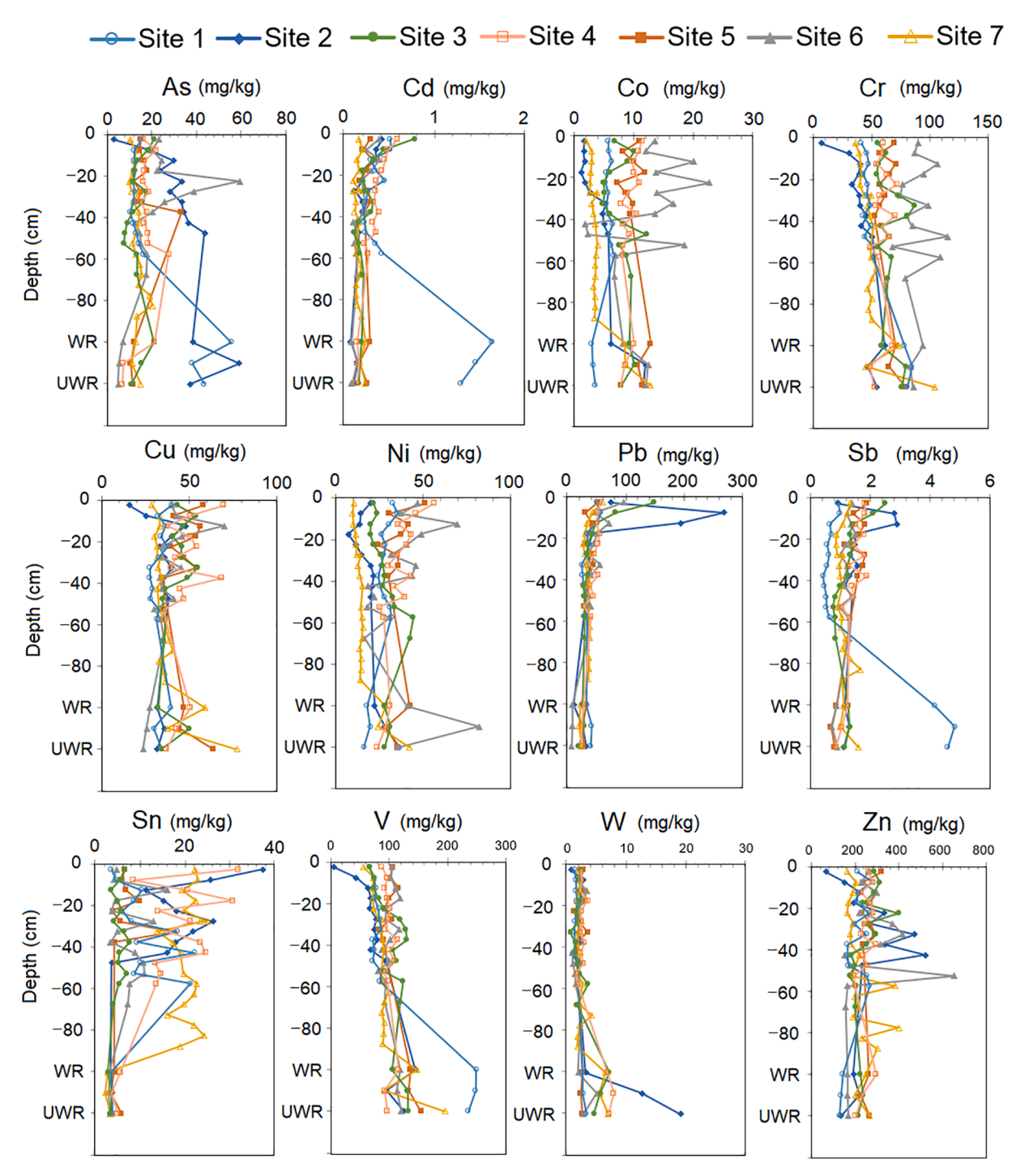


Fig. 3. Total TMM concentrations for soil profiles and rock samples (weathered, unweathered) for each site.

and soil properties were explored with linear regressions in Supplemental Table 3. Total concentrations of Fe, Co, Cr, and Ni were positively correlated (R > 0.5, p < 0.05). Similarly, total concentrations of Cd, V, and Sb were positively correlated (R > 0.5, p < 0.05). Soil pH was not significantly correlated with any total TMM concentration but %LOI was positively correlated with total Sb concentrations (R > 0.5, p < 0.05). MAT was positively correlated with the average total Cr and Co concentrations in the soil profile (R > 0.5, p < 0.05) but negatively correlated with total As, Cd, Cr, Ga, Sn, Sb, Pb, and V (R \leq - 0.5, p < 0.05). MAP was not positively correlated with any total TMM concentrations but was negatively correlated with total Ni, Ga, Cd and soil pH (R \leq - 0.5, p < 0.05).

Tau values were determined for TMMs by indexing their soil concentrations relative to Ti in each soil depth compared with ratios in the unweathered shale bedrock to determine the extent of enrichment and depletion (Fig. 3). Broadly speaking, there were four general trends observed for the different TMMs. First, their tau values for As, Cd, and Sb show enrichment or minimal depletion at all sites except Site 1, which had substantial depletion (Fig. 3). Second, there was site specific trends, in which tau values for Co, Cu, and Ni show mixed enrichment and depletion across sites (Fig. 3). Only consistent depletion at Site 7 and consistent enrichment at Sites 1 and 4 were consistent across Co, Cu, and Ni. Third, there were consistent depletion, indicated by the negative tau values for Cr, W and V across all sites (Fig. 3). Lastly, some TMMs were

broadly enriched across all sites for most depths in the soil profile, which was the case indicated by tau values for Pb, Sn, and Zn.

3.3. Oxidizable and reducible TMM phases

We determined the importance of organic matter in TMM sequestration, the first step of the sequential extraction utilized 30% H₂O₂ to dissolve oxidize organic matter, releasing organic-complexed TMMs. The data in Table 2 shows that oxidizable fraction of TMMs was limited, making up < 5% of total Fe, As, Cr, Cu, Ga, Pb, Sn, Sb, V, and Zn concentrations in shales studied. The oxidizable fraction of Cd, Ni, and W were also small, comprising 1-16% of their total concentration in bedrock shale samples. At Site 1, the oxidizable fraction of Co was 52%of the total Co concentration, which was anomalous compared to 1-5% for the other six sites. Similar to rocks, Table 3 shows that the oxidizable fraction of TMMs was very limited, making up < 5% of total Fe, As, Cr, Cu, Ga, Ni, Pb, Sn, Sb, V, W, and Zn concentrations in shales studied. The oxidizable fraction of Cd and Co were also small, comprising 1-14% of their total concentration in bedrock shale samples. Oxidizable concentrations of Cu, Zn, Ga, As, Cd, Sn, Sb, V, Cr, Pb, and Fe were all positively correlated with each other (R > 0.5, p < 0.05, Supplemental Table 1). Soil pH and LOI were not correlated with any oxidizable TMM concentrations. Lastly, the relationship between climate and soil properties with oxidizable TMM concentrations was explored with linear regressions (Supplemental Table 4). Oxidizable concentrations of Ga, As, Cd, and Pb were negatively correlated with MAT (R > 0.5, p < 0.05). Oxidizable Cd concentrations were negatively correlated with MAP (R > 0.5, p < 0.05).

In addition to organic matter, oxyhydroxides and sulfidic minerals can affect TMM sequestration. Thus, the second step of the sequential extraction utilized citrate-bicarbonate-dithionite (CBD) to dissolve oxyhydroxides (primarily Fe) using strong reducing conditions to releasing oxide-complexed TMMs. Table 4 shows that reducible fraction was a notable proportion of many TMMs in the shale bedrock, making up 5–50% of the total concentration of all metals except for Cr which was only 3-7% (Table 5). Soil reducible fraction of TMMs was a larger proportion of the total TMM concentrations than for the shale bedrocks. The soil reducible fraction made up 10-60% of the total concentration of Fe, As, Cd, Co, Cu, Ni, Sb, Sn, V, W, and Zn (Table 5). Reducible fraction of Cr and Pb were only 5-21% of their total concentrations (Table 5). Gallium was an exceptional case as < 2% was in the reducible soil and rock fractions, indicating it was exclusively associated with aluminosilicates. Lastly, the relationship among reducible TMM concentrations with climate and soil properties was explored using linear regressions (Supplemental Table 2). Reducible concentrations of Cr, Cu, Ni, Zn, As, Sb, and Fe were all positively correlated (R > 0.5, p < 0.05). Soil pH was positively correlated with reducible Co and Ni concentrations but LOI was not correlated with any reducible TMM concentrations. Reducible concentrations of As, Fe, Cr, and Co were positively correlated with MAT but reducible Ga, As, Cd, and Pb were negatively correlated with MAT (R > 0.5, p < 0.05). Reducible Cd concentrations were negatively correlated with MAP (R > 0.5, p < 0.05).

3.4. Shale mineralogical analyses

Mineralogy of all unweathered (UWR) shale samples was dominated (63 to 85% total composition) by quartz and plagioclase feldspar (Fig. 5A and B). The rest of the soil mineralogy was dominated by mica (characterized by a 10 Å peak), chlorite (peaks at 14 Å and 7 Å), and kaolinite (7 Å peak). Site 2 contained quantifiable calcite at 3% but was undetectable in UWR shale samples across the seven sites. Sulfides (pyrite, pyrrhotite, galena, etc) and Fe oxides (hematite, geothite, etc) were not detected or quantified by XRD in any UWR shale samples across the seven sites. However, poorly crystalline and amorphous oxides are likely present but did not exhibit enough crystallinity to be identified and quantified by XRD. The types of phyllosilicates present were determined by comparing air-dried, ethylene glycol solvated and, 400 °C heated patterns for each sample (Moore and Reynolds, 1997). Except for the Site 3 UWR shale, specific clay treatments (Supplemental Fig. 1), did not show significant peak shifting following ethylene glycol solvation and heating at 400 °C, confirming the attribution of the 14 Å peak to chlorite, the presence of mica and the presence of kaolinite in all samples. The phyllosilicate clay mineralogy for the Site 3 UWR shale showed a collapse of the 14 Å peak to 10 Å indicative that the 14 Å peak is attributable to vermiculite.

3.5. Batch reactor experiments-Solution changes and TMM releases

Batch reactors were conducted to explore the release mechanism of TMMs from unweathered shale from Site 1 over 7 days of dissolution. First, most treatments had a 0.1–0.4 pH unit change. Control, Treatment 1, Treatment 5 had decreases of 0.2 to 0.4 pH units (Table 6). Treatment 2, Treatment 3, and Treatment 4 had pH increases of 0.2 to 0.3 pH units (Table 6). Treatments 6 and 7 with the dithionite treatments had the largest pH shifts, with decreases of 0.8 and 0.9, respectively. The highest dissolution rates for Al, K and Si occurred under Treatments 3 and 4, under oxic conditions with organic acids and acidic conditions of pH 4.1 and 5.9. The release of Fe was greatest under reducing conditions, slightly acidic solutions of Treatment 6. However, Fe release under oxic acidic conditions with organic acids in Treatment 3 was also two orders of magnitude higher than the control. Interestingly, Ca dissolution was greatest under the control and acidic reducing treatments.

TMM release varied widely among the treatments but was categorized into two groups, TMMs with greatest release rates under reducing conditions and TMMs released under oxic, acidic conditions with organic acids. Under the first grouping, As, Cd, Co, Cu, Ni, V, and Zn had the highest dissolution rates under reducing conditions of Treatments 6 and 7 (Table 7), with their release rates were 3 to 150 times faster than the control treatment. Of those metals, As, Co, Cu, Ni, and V had greatest dissolution rates under basic (pH 8.1), reducing solutions while Cd, Pb, and Zn had higher dissolution rates under acidic (pH 5.9), reducing conditions (Table 7). In the second group of metals, Cr, Sn, Sb, and W had their highest dissolution rates under oxic, acidic conditions of pH 4.1 and 5.9 with organic acids (Table 7). Under oxic, acidic, organic acid conditions, their dissolution rates increased by 4 to 48 times compared to the control treatment.

Table 2Mean oxidizable rock fraction of the total TMM concentration.

	Fe	As	Cd	Co	Cr	Cu	Ga	Ni	Pb	Sb	Sn	V	W	Zn
	%	%	%	%	%	%	%	%	%	%	%	%	%	%
Site 1	1	0	5	52	0	2	0	8	0	1	2	1	12	2
Site 2	0	0	2	1	0	0	0	1	0	0	2	0	16	0
Site 3	0	0	6	5	0	1	0	3	1	0	2	1	4	0
Site 4	0	0	2	3	0	0	0	2	0	0	2	0	12	0
Site 5	0	0	1	2	0	1	0	1	0	0	1	0	7	0
Site 6	0	1	9	3	0	1	0	1	1	1	2	2	6	0
Site 7	0	0	1	3	0	0	0	2	0	0	2	0	7	0

Table 3Mean oxidizable soil fraction of the total TMM concentration.

	Fe	As	Cd	Co	Cr	Cu	Ga	Ni	Pb	Sb	Sn	V	W	Zn
	%	%	%	%	%	%	%	%	%	%	%	%	%	%
Site 1	0	0	5	5	0	1	0	2	0	1	1	1	1	0
Site 2	3	1	12	14	1	2	1	3	1	2	1	2	2	2
Site 3	0	0	9	14	0	1	0	1	1	1	1	1	1	1
Site 4	0	0	2	3	0	1	0	3	0	0	0	1	0	0
Site 5	0	0	3	8	0	1	0	2	0	0	2	1	1	0
Site 6	0	0	4	9	0	0	0	1	0	0	1	0	0	0
Site 7	0	0	5	5	0	0	0	1	0	0	0	0	0	1

Table 4Mean rock reducible (Citrate-bicarbonate-dithionite) fraction of the total TMM concentration.

	Fe	As	Cd	Co	Cr	Cu	Ga	Ni	Pb	Sb	Sn	V	W	Zn
,	%	%	%	%	%	%	%	%	%	%	%	%	%	%
Site 1	45	11	23	37	7	39	0	29	6	16	46	13	71	20
Site 2	22	9	27	54	4	37	0	13	13	7	69	7	55	10
Site 3	44	19	27	83	7	42	0	18	11	24	38	16	91	15
Site 4	45	11	67	74	8	36	0	20	9	20	90	19	66	20
Site 5	14	4	14	45	3	21	0	6	17	19	81	5	63	5
Site 6	10	5	25	32	5	77	0	13	55	16	82	35	84	52
Site 7	43	13	21	56	7	39	0	23	12	30	77	16	67	13

Table 5Mean soil reducible (Citrate-bicarbonate-dithionite) fraction of the total TMM concentration.

	Fe	As	Cd	Co	Cr	Cu	Ga	Ni	Pb	Sb	Sn	V	W	Zn
	%	%	%	%	%	%	%	%	%	%	%	%	%	%
Site 1	57	28	38	67	12	55	0	13	21	33	43	41	54	30
Site 2	51	30	31	63	18	54	1	16	13	23	45	57	54	33
Site 3	63	17	41	57	8	38	0	15	9	22	56	25	51	15
Site 4	41	12	37	61	6	31	1	17	9	14	32	16	27	15
Site 5	50	17	35	61	9	29	0	16	10	20	43	24	67	12
Site 6	47	14	22	33	8	52	0	6	5	20	55	38	32	31
Site 7	60	31	34	39	15	59	0	16	5	25	40	33	53	17

Table 6 Macroelements released and solution pH over 7 d batch reactor experiment using Site 1 unweathered shale. N = 6 for each treatment.

Treatment	Redox	Organic acids	Starting pH	Final pH	Al	Fe	K	Ca	Si
					μg	μg	mg	μg	μg
Control	Oxic	None	5.8	5.2	41	13	1.5	440	144
Treatment 1	Oxic	None	4.4	4.2	127	24	1.7	404	132
Treatment 2	Oxic	None	8.1	8.3	8	30	2.7	218	249
Treatment 3	Oxic	Added	4.1	4.4	541	4757	2.9	52	360
Treatment 4	Oxic	Added	5.9	6.1	428	1532	3.8	90	786
Treatment 5	Oxic	Added	8.3	8.2	152	285	2.1	168	446
Treatment 6	Reduced	None	6.5	5.7	14	16,870	1.2	450	285
Treatment 7	Reduced	None	8.2	7.3	2	2971	1.4	321	239

Table 7 TMMs released to solution over 7 d batch reactor experiment using Site 1 unweathered shale. N=6 for each treatment. Treatments with the highest dissolution are bold.

Treatment	Redox	Organic acids	Starting pH	As	Cd	Cr	Co	Cu	Ga	Ni	Pb	Sn	Sb	V	W	Zn	Ga/Al
				μg	ng	ng	ng	μg	ng	ng	ng	ng	ng	μg	ng	ng	mmol/mol
Control	Oxic	None	5.8	1.0	4	10	70	18	0.5	201	3	9	5	30	5	62	0.005
Treatment 1	Oxic	None	4.4	1.2	3	15	122	25	0.4	266	6	9	5	38	4	173	0.001
Treatment 2	Oxic	None	8.1	0.4	10	8	1	13	0.3	39	0.4	8	30	13	9	1	0.015
Treatment 3	Oxic	Added	4.1	1.0	40	168	57	9	20.1	112	18	27	218	19	45	59	0.014
Treatment 4	Oxic	Added	5.9	0.8	18	121	97	37	9.6	145	6	34	121	25	68	165	0.009
Treatment 5	Oxic	Added	8.3	0.6	12	48	18	42	0.8	99	1.5	26	52	19	33	5	0.002
Treatment 6	Reduced	None	6.5	4.3	76	47	167	1	8.8	514	449	4	66	2	17	1527	0.239
Treatment 7	Reduced	None	8.2	4.5	12	56	455	94	1.3	983	23	33	19	139	14	635	0.281

3.6. Gallium-Aluminum ratios

Total Ga concentrations ranged from 14 to 49 mg/kg with an average of 24.7 \pm 0.6 mg/kg across all rocks and soils. Total Ga concentrations were largely comparable throughout the weathering profile, but Sites 4, 5, and 6 had higher total Ga concentrations than Sites 1 and 2 (Supplemental Fig. 3). Oxidizable Ga concentrations were very low compared to total and reducible concentrations, ranging from 0.001 to 0.451 mg/kg with an average of 0.043 \pm 0.008 mg/kg across all rocks and soils (Supplemental Fig. 3). Reducible Ga concentrations were also much lower than total Ga concentrations, ranging from 0.07 to 2.71 mg/kg with an average of 0.79 \pm 0.04 mg/kg across all rocks and soils. Reducible Ga was present throughout the weathering profile, but much

lower in the weathered and unweathered rock (Supplemental Fig. 3). The Ga/Al ratio for the oxidizable fraction was 0.26 ± 0.03 mmol/mol, which was higher and more variable than total range of Ga/Al being 0.15 ± 0.01 mmol/mol but the Ga/Al ratio in the reducible fraction $(0.13\pm0.01$ mmol/mol) was largely comparable with the total Ga/Al. Gallium and Al were significantly correlated with each other in the oxidizable fraction (R=0.72, p<0.05), in the reducible fraction (R=0.62, p<0.05), and in the total digests (R=0.51, p<0.05). Total Ga/Al ratios were 0.15 ± 0.01 mmol/mol, which was slightly higher than in USGS rock standards 0.07 to 0.12 mmol/mol.

Lastly, we examined the release of Ga and Ga/Al ratios in the weathering in the batch reactor experiment (Table 7). Gallium dissolution was greatest under oxic, acidic conditions with organic acids. But

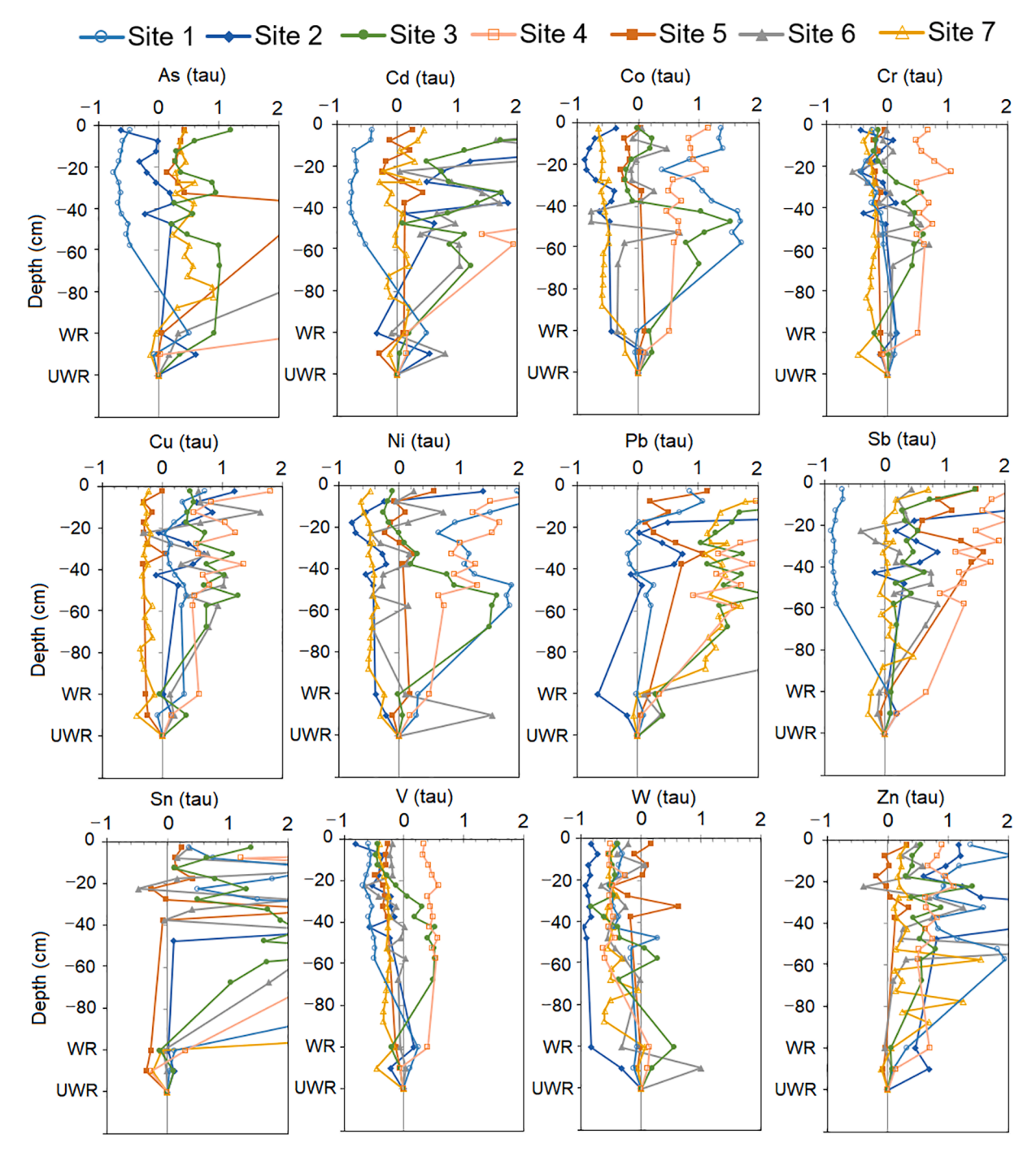


Fig. 4. TMM tau values for each soil horizon using the unweathered rock samples as the parent material and Ti as the reference element.

slightly acidic solutions under both oxic and reduced conditions produced similar Ga dissolution rates. Oxic conditions generated very low Ga/Al ratios (0.001–0.01 mmol/mol) while reduced conditions generated comparable Ga/Al ratios (0.24–0.28 mmol/mol) compared with in the initial Site 1 unweathered rock of 0.21 mmol/mol.

4. Discussion

4.1. Accumulation and release of TMMs from shales

Our results show that trace metal and metalloid (TMM) concentrations are generally below concentrations that pose hazards to plants, animals, and humans both within the grey shales studied and in their overlying soils. Only As and Pb had concentrations exceeding United States Environmental Protection Agency (USEPA) soil screening levels that can be toxic to plants or animals of > 18 mg/kg and > 120 mg/kg, respectively. The soils and rocks studied here were grey shales that did not have toxic concentrations typically observed in the organic-rich black shales, which can have much higher trace metal concentrations as shown in black shales by Perkins and Mason (2015), Raiswell and Plant (1980), and Gregory et al., (2015).

The Tau values showed that shale-derived soils were net

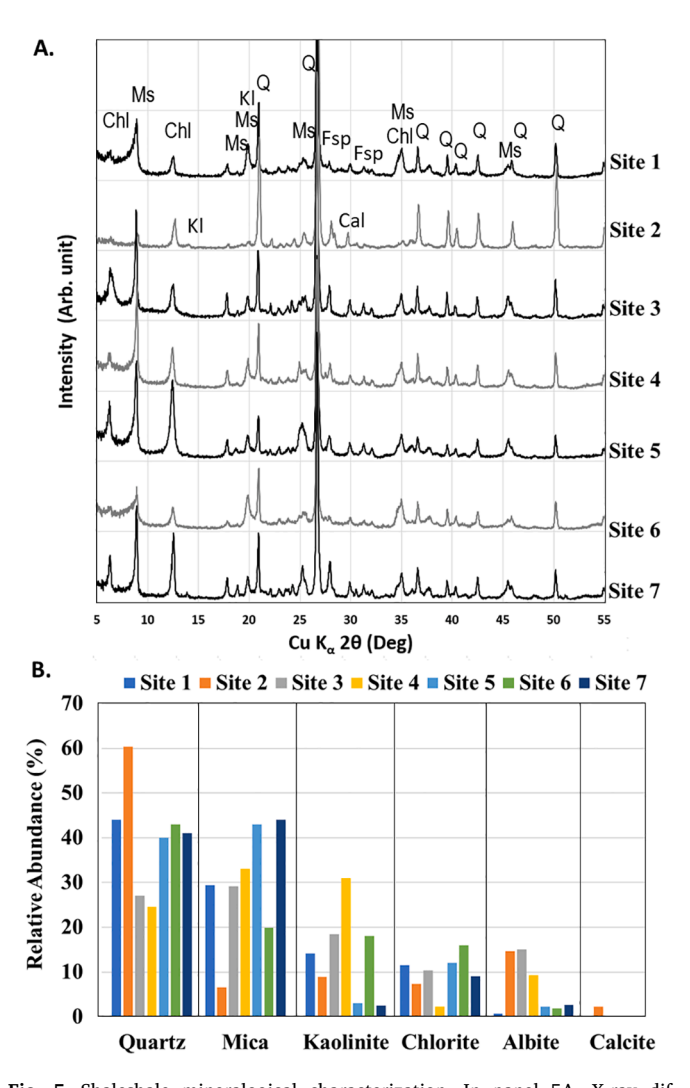


Fig. 5. Shaleshale mineralogical characterization. In panel 5A, X-ray diffractograms of the various shale samples, letters identify mineral phase peaks (Q = Quartz, Ms = Muscovite (Mica) , Kl = Kaolinite, Chl = Chlorite, Fsp = Feldspar (albite, orthoclase), Cal = Calcite). In panel 5B, Relative abundance of X-ray quantified mineral phases are shown.

accumulators for many of the TMMs (As, Cd, Co, Cu, Ni, Pb, Sb, Sn and Zn) across most sites (Fig. 4). We hypothesize that these added metals are primarily retained in the reducible fraction (neoformed or inherited oxides) of soils as opposed to the oxidizable fraction (organic matter). First, oxidizable soil TMM fractions were largely comparable with their respective oxidizable rock TMM fraction for metals that had net accumulation in the soil (Tables 2 and 3). Second, the oxidizable soil TMM concentrations were very low and total concentrations of the indexing element Ti concentrations remained relatively high suggesting addition from the atmosphere or biological cycling rather than inheritance from the grey shale bedrock. Third, the soil reducible TMM fractions were greater than the rock reducible TMM fractions for nearly all of the depths exhibiting net accumulation (As, Cd, Cu, Sb, and Zn) suggesting net addition to the reducible fraction. All of these lines of evidence suggest many of the TMMs (As, Cd, Co, Cu, Ni, Pb, Sb, Sn and Zn) were net accumulated in the shale-derived soils from the atmosphere or surficial cycling, in secondary oxides that were either inherited or neoformed (discussed later). Other TMMs (Cr. W. and V) did not exhibit accumulation and were either retained or lost from the profile during weathering on the basis of largely negative or near zero tau values and concentrations that did not increase with depth. Most interestingly, these are TMMs that exist as hydroxyanions or oxyanions (commonly HCrO₄⁻¹ or Cr(OH)₄⁻¹, WO₄⁻², and VO₃⁻¹) (Kabata-Pendias and Szteke, 2015), for which their negative charged species can enhance their mobility in soil. Anion exchange capacity was not accessed in these soils, thus their relative mobility and the soil sorption capacity cannot be compared or discussed. From our weathering profiles, our extractions showed that neoformed reducible fractions (Fe oxides) are important for accumulating TMMs during weathering or from aboveground cycling or inputs.

The grey shale soil with the highest TMM concentrations was weathered under laboratory conditions to explore the aqueous conditions that promote TMM release from shale over 7 d (Table 7). Our results confirmed that the reducible fraction (comprised of an undetermined mixture of Fe oxides) was most important for the release of many TMMs (As, Cd, Co, Cu, Ni, Pb, V, and Zn) from shale (Table 4 and 5). Iron dissolution was greatest under reduced, slightly acidic conditions. Reduced basic conditions were two orders of magnitude greater than non-organic acid treatments (Table 7). However, several TMMs (Cr, Ga, Sn, Sb, and W) also had their highest release rate under oxic, acidic conditions with organic acids. This suggests that they are likely sourced from aluminosilicate dissolution, most likely phyllosilicates, as Al and Si dissolution was greatest under those conditions (Table 6). However, the second highest Fe release also occurred under oxic, acidic conditions with organic acids (Table 6), which may be due to oxidation and organic acid mediated dissolution of reduced Fe minerals like pyrite (Mahoney et al., 2019). While previous studies have observed the wide abundance of TMMs within the pyrite in shales (e.g. Raiswell and Plant, 1980; Zhu et al., 2008), the absence of detectable crystalline pyrite in the parent shale suggests that this Fe was associated with poorly crystalline or amorphous phases.

4.2. TMMs and soil development from shale across climates

We expected the pedogenic development and physicochemical properties of the shale-derived soils to follow general trends along the north–south climate-pedogenesis gradient, but instead localized effects substantially impacted the soils. Organic matter accumulation in the surface horizons did not correspond with the climate-pedogenesis gradient (Fig. 2). Younger, cooler sites did not have significantly higher %LOI than older, warmer soils. It is typically generalized that warmer soils result in greater carbon loss from soil (e.g. Melillo et al., 2017); however, more localized effects such as bioturbation (e.g. White and Dere, 2014), topographic, and geomorphic processes (e.g. Román-Sánchez et al., 2018) can affect carbon and organic matter storage. We also expected soil chemistry such as macroelements and base saturation

to decrease along the climate-pedogenesis gradient (Fig. 2 and Supplemental Fig. 2). Instead, Site 2 exhibited very low substantial base cations and was classified as an Ultisol instead of an Alfisol and the two middle sites, Sites 4 and 5, had the highest base saturation. Further, we expected lower Al, Fe, K, and Na concentrations in the warmer sites than the cooler sites due to weathering during pedogenesis, but this was not clearly observed. We did observe lower Na tau values with soil development as the colder Sites 1, 2, 3, and 4 had more Na than warmer sites 5, 6, and 7 (Supplemental Fig. 2). However, soils at all sites exhibited similar patterns of K depletion and accumulation of Al and Fe as shown with tau values. Thus, the soils are undergoing pedogenesis, but we expected greater Al, Fe, K, and Na loss at Ultisols than Alfisols and that this was not observed.

Instead, the climate-pedogenesis gradient of shale-derived soils appear to be influenced by local geomorphic processes. The soils we sampled are on upland hillslopes, which as described in Sobecki and Karathanasis (1992), can still be impacted by colluvium mixing and parent material discontinuities. We attempted to limit these effects using singular weathering profiles that did not exhibit textural differences. However, Sobecki and Karathanasis (1992) noted this mixing of materials and discontinuities could result in higher-than-expected base cations (like Ca) and weathering discontinuities. This may alternatively explain the higher-than-expected Al, Fe, and K concentrations and potentially some of the large differences in TMM concentrations between soil and unweathered bedrock (Supplemental Fig. 2). Moreover, this may explain why TMM concentrations did not vary with climate or extent of pedogensis; cooler, younger soils (Site 1, 2, 3, and 4) did not have contrasting TMM concentrations than warmer, older soils (Sites 5, 6, and 7). However, field methods used, and localities sampled should have minimized this mixing effect within each individual weathering profile. Differences along the climatic gradient and corresponding changes in expected pedogenic development were masked (particularly Site 2, 4, and 5) by colluvium, localized parameters such as shale composition, proximity to human pollution sources, hydrologic features not explored here, or vegetation were likely most important for TMM accumulation and release.

4.3. Ga/Al Ratios

We examined Ga/Al ratios as a method to explore aluminosilicate weathering patterns of incongruent precipitation of new oxide or clay minerals or congruent release. Our field soil extractions show that Ga and Al were positively, moderately correlated across oxidizable, reducible, and total concentrations (Supplemental Tables 1–3),

demonstrating their similar biogeochemistry. Moreover, younger less weathered Alfisols exhibited Ga/Al ratios (0.12 to 0.18 mmol/mol) similar to more extensively weathered Ultisols (0.12-0.18 mmol/mol) (Table 1, Fig. 6). This comparability between Ga/Al ratios in Alfisols and Ultisols suggest that across the sites pedologic histories and current weathering intensities, aluminosilicate dissolution has not significantly fractionated the Ga/Al ratio (Fig. 6). Furthermore, our results demonstrate the tight linkage between Ga and Al (Supplemental Tables 1–3). The soil oxidizable fraction had the widest variation in Ga/Al ratios, with low values of 0.02-0.04 mmol/mol at Site 7 from low Ga (<0.002 mg/kg) and high values at Sites 4 and 5 of 0.13 to 1.46 mmol/mol from low Al retention. One hypothesis is that the difference is driven by pHcontrolled organic ligand complexation. Gallium and Al are sorbed to organic matter at different rates due to slight differences in their point of zero charge and pH of dissociation (Shiller and Frilot, 1996; Hieronymus et al., 2001). Average soil pH were highest at Sites 4 and 5 (pH 6.0-6.5) compared to the other sites (pH 3.1-5.2) (Fig. 2). At higher pH Al is neutral or positively charged (Al(OH)₂⁺¹ or Al(OH)₃) while Ga is predominately negatively charged (Ga(OH)₄⁻¹), allowing for great Al sorption to negatively charged dissolved organic ligands. However, total Ga concentrations in the oxidizable phase is a small proportion of the total Ga concentration and unlikely to be a key Ga/Al phase produced during aluminosilicate weathering. The results from the batch reactor experiments showed that oxic, non-organic rich solutions as well as basic conditions with organic ligands generated low Ga/Al ratios (0.02-0.09 mmol/mol). Mineral dissolution resulting in a solution with low Ga/Al ratio (0.02 to 0.09 mmol/mol; Table 7) should eventually lead to a solid phase with a higher Ga/Al ratio (>0.18 mmol/mol). Comparing the batch reactor results with our solid phase field results suggests that shale weathering is driven by a pathway that does not fractionate Ga/Al ratio, such as dissolution by organic ligands under acidic conditions or production of colloids with similar Ga/Al ratios. Few studies have examined Ga/Al ratio in terrestrial systems but one key study by Shiller and Frilot (1996) observed stream water with very high Ga/Al ratios (0.17–1.78 mmol/mol) in slightly basic Californian stream waters which generated lower Ga/Al ratios in soil (0.06-0.10 mmol/ mol) than underlying bedrock (0.04-0.34 mmol/mol). Thus, further research using in-situ and ground and stream water samples from the watersheds are needed to determine the export Ga/Al ratios. Stream water samples were collected in this study but were unusable due to improper storage.

Our Ga/Al ratio results in field samples and laboratory conditions suggest organic compounds and other processes that do not fractionate the Ga/Al ratio play key roles in shale weathering with some

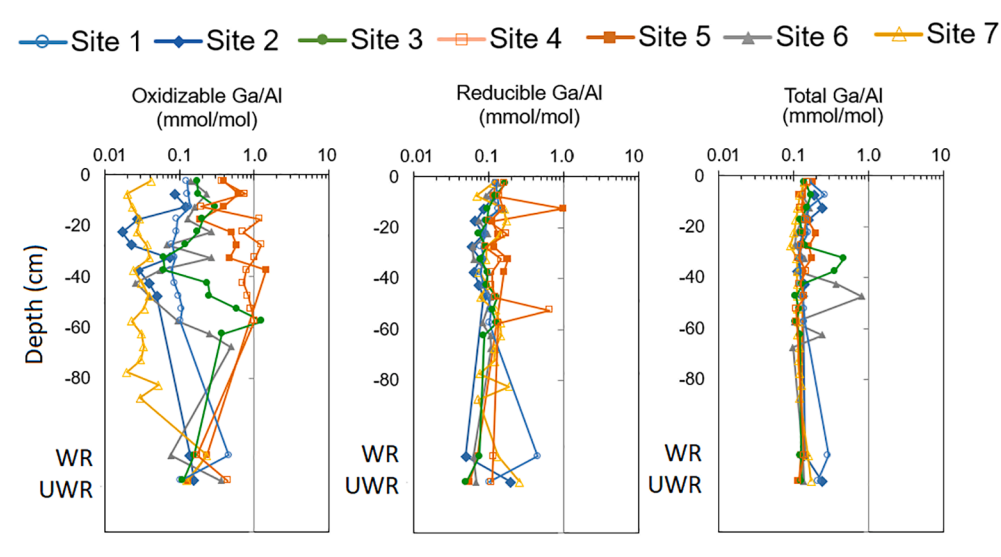


Fig. 6. GA/Al ratios were calculated for each soil and rock sample across the seven sites.

implications for TMM retention and mobilization. The sorption of TMMs to organic acids may be the dominant process governing their retention in the soil profile, following TMM addition by humans and aboveground cycling. Other processes such as colloid production may also govern if TMMs are retained in soil profiles or leached out. As described by Aguirre et al., (2017), the composition of colloids changes with sources, as base flow colloids, erosional colloids, and human generated colloids have different Al and Fe composition which can alter TMMs transport from soil to rivers..

5. Conclusions and future research needs

Overall, TMM concentrations in the grey shales and their soils were below concentrations known to be toxic and below concentrations observed in black shales, except for As and Pb at two sites. Tau values showed that shale-derived soils are net accumulators of many TMMs (As, Cd, Co, Cu, Ni, Pb, Sb, Sn and Zn). Many of the TMMs had high proportions that were sequestered in reducible phases (amorphous and poorly-crystalline Fe oxides) at rates higher than in their shale bedrock, but few TMMs were in oxidizable phases (organic matter). TMM accumulation and release during weathering was not extensively related to climate or soil development/age, as we hypothesized localized effects of vegetation, geomorphology, pollution, and physicochemical parameters of the shale masked most regional effects, even for most macro elements except Na.

Our laboratory batch reactor experiments indicate that greatest TMMs release can occur under oxic, acidic conditions with organic acids present for some TMMs (Cr, Ga, Sn, Sb, and W) while other TMMs had their highest release via slightly acidic, reduced conditions (As, Cd, Co, Cu, Ni, Pb, V, and Zn). This suggests that some TMMs are dominated by aluminosilicate dissolution while others are controlled by complexation with geogenic Fe oxides. We explored Ga/Al ratios to better understand the mechanism driving aluminosilicate dissolution and total Ga/Al ratios were not different across the climate-soil development gradients. Our batch reactor experiments showed oxic, acidic conditions with organic ligands present can release Ga and Al to solution without fractionating the Ga/Al ratios. This implies weathering of shales is dominated by processes that may not fractionate Ga/Al ratio (due to organic ligands or potentially colloids).

Our study is another step forward in understanding the impact of shale weathering on terrestrial environments and there are several foci areas for future research. The lack of surface or groundwaters limits our ability to understand the implications at the watershed scale, but we can hypothesize that shale-derived soils are impacting watershed-scale biogeochemistry by retaining TMMs, they can be active sources for others (specifically Cr, V, W). Further studies are needed to examine more specific minerals or soil phases (e.g. organic vs sulphides) that are holding the TMMs. Our extractions were broad investigations and we could not quantify geogenic Fe oxides and neoformed Fe oxides, and all three phases can be important sources and sinks of TMMs. Further microscale examinations of Fe oxide (e.g. Mahoney et al., 2019; Li et al., 2020) are needed to examine changes in TMM sorption and their relationship with geogenic and neoformed Fe oxides . Moreover, stable isotopes can be applied to several of TMMs to determine if the enrichment observed by tau values are from human pollution (such as Pb) or long-term retention from geogenic Fe oxides.

Declaration of Competing Interest

The authors declare that they have no known competing financial interests or personal relationships that could have appeared to influence the work reported in this paper.

Acknowledgements

We thank Sumaya Hamdi and Corey Palmer for site selection and

collecting the soil and rock samples, Mark Butler, Ainsley McStay, and Eliza Fitzgerald for processing the soil and rock samples and conducting the digestions and extractions. This project was funded by a grant from the United States National Science Foundation Award #1660923 to Louis Derry and subaward to Dr. Justin Richardson and additional funding from the University of Massachusetts Amherst College of Natural Sciences to Dr. Justin Richardson.

Appendix A. Supplementary data

Supplementary data to this article can be found online at https://doi.org/10.1016/j.geoderma.2021.115431.

References

- Adriano, D.C., 2001. Trace Elements in Terrestrial Environments. Springer, New York, NY.
- Aguirre, A.A., Derry, L.A., Mills, T.J., Anderson, S.P., 2017. Colloidal transport in the Gordon Gulch catchment of the Boulder Creek CZO and its effect on C-Q relationships for silicon. Water Resour. Res. 53 (3), 2368–2383.
- Anderson, S.P., Dietrich, W.E., Brimhall Jr, G.H., 2002. Weathering profiles, mass-balance analysis, and rates of solute loss: Linkages between weathering and erosion in a small, steep catchment. Geol. Soc. Am. Bull. 114 (9), 1143–1158.
- Brimhall, G.H., Dietrich, W.E., 1987. Constitutive mass balance relations between chemical composition, volume, density, porosity, and strain in metasomatic hydrochemical systems: results on weathering and pedogenesis. Geochim. Cosmochim. Acta 51, 567–587.
- Ciolkosz, E.J., Waltman, W.J., Simpson, T.W., Dobos, R.R., 1989. Distribution and genesis of soils of the northeastern United States. Geomorphology 2 (1–3), 285–302.
- Ciolkosz, E.J., Carter, B.J., Hoover, M.T., Cronce, R.C., Waltman, W.J., Dobos, R.R., 1990. Genesis of soils and landscapes in the Ridge and Valley province of central Pennsylvania. Geomorphology 3 (3–4), 245–261.
- Dere, A.L., White, T.S., April, R.H., Reynolds, B., Miller, T.E., Knapp, E.P., McKay, L.D., Brantley, S.L., 2013. Climate dependence of feldspar weathering in shale soils along a latitudinal gradient. Geochim. Cosmochim. Acta 122, 101–126.
- Dere, A.L., White, T.S., April, R.H., Brantley, S.L., 2016. Mineralogical transformations and soil development in shale across a latitudinal climosequence. Soil Sci. Soc. Am. J. 80 (3), 623–636.
- Fu, X., Wang, J., Tan, F., Feng, X., Zeng, S., Chen, W., Wang, D., 2015. Minerals and potentially hazardous trace elements in marine oil shale: new insights from the Shengli River North surface mine, northern Tibet, China. Environ. Earth Sci. 73 (7), 2127, 2157.
- Gee, G.W., Bauder, J.W. and Klute, A., 1986. Methods of soil analysis, part 1, physical and mineralogical methods. Soil Science Society of America, American Society of Agronomy.
- Gregory, D.D., Large, R.R., Halpin, J.A., Baturina, E.L., Lyons, T.W., Wu, S., Danyushevsky, L., Sack, P.J., Chappaz, A., Maslennikov, V.V., Bull, S.W., 2015. Trace element content of sedimentary pyrite in black shales. Econ. Geol. 110 (6), 1389–1410.
- Herndon, E.M., Brantley, S.L., 2011. Movement of manganese contamination through the Critical Zone. Appl. Geochem. 26, S40–S43.
- Hieronymus, B., Kotschoubey, B., Boulègue, J., 2001. Gallium behaviour in some contrasting lateritic profiles from Cameroon and Brazil. J. Geochem. Explor. 72 (2), 147–163.
- Hosterman, J.W., Whitlow, S.T., 1981. Clay mineralogy of devonian shales in the appalachian basin. Geol. Surv. Open-File Rep. (US);(United States) 81.
- Jin, L., Ma, L., Dere, A., White, T., Mathur, R., Brantley, S.L., 2017. REE mobility and fractionation during shale weathering along a climate gradient. Chem. Geol. 466, 352–379.
- Kabata-Pendias, A., Szteke, B., 2015. Trace Elements in Abiotic and Biotic Environments. CRC Press.
- Kurtz, A.C., Derry, L.A., Chadwick, O.A., Alfano, M.J., 2000. Refractory element mobility in volcanic soils. Geology 28 (8), 683–686.
- Li, Q., Zhu, B., Li, J., 2020. A comparative study on the micro-surface characteristics at black shale initial oxidation stage. Sci. Rep. 10 (1), 1–9.
- Liu, Y., Xiao, T., Perkins, R.B., Zhu, J., Zhu, Z., Xiong, Y., Ning, Z., 2017. Geogenic cadmium pollution and potential health risks, with emphasis on black shale. J. Geochem. Explor. 176, 42–49.
- Lyons, W.B., Fitzgibbon, T.O., Welch, K.A., Carey, A.E., 2006. Mercury geochemistry of the Scioto River, Ohio: impact of agriculture and urbanization. Appl. Geochem. 21 (11), 1880–1888.
- Ma, L., Konter, J., Herndon, E., Jin, L., Steinhoefel, G., Sanchez, D., Brantley, S., 2014.Quantifying an early signature of the industrial revolution from lead concentrations and isotopes in soils of Pennsylvania, USA. Anthropocene 7, 16–29.
- Mahoney, C., März, C., Buckman, J., Wagner, T., Blanco-Velandia, V.O., 2019. Pyrite oxidation in shales: Implications for palaeo-redox proxies based on geochemical and SEM-EDX evidence. Sed. Geol. 389, 186–199.
- Mehra, O.P. and Jackson, M.L., 2013. Iron oxide removal from soils and clays by a dithionite-citrate system buffered with sodium bicarbonate. In Clays and clay minerals (pp. 317-327). Pergamon.
- Melillo, J.M., Frey, S.D., DeAngelis, K.M., Werner, W.J., Bernard, M.J., Bowles, F.P., Pold, G., Knorr, M.A., Grandy, A.S., 2017. Long-term pattern and magnitude of soil

- carbon feedback to the climate system in a warming world. Science 358 (6359), 101-105.
- Moore, D.M., Reynolds, R.C., 1997. X-Ray Diffraction and the Identification and Analysis of Clay Minerals. Oxford Univ, Press.
- National Oceanographic and Atmospheric Administration (NOAA) (2011) Climate Data Online: Monthly Observational Data. U.S. Department of Commerce, National Oceanic and Atmospheric Administration, National Environmental Satellite Data and Information Service, National Climatic Data Center. http://www.ncdc.noaa.gov/cd
- Perkins, R.B., Mason, C.E., 2015. The relative mobility of trace elements from short-term weathering of a black shale. Appl. Geochem. 56, 67–79.
- Raiswell, R., Plant, J., 1980. The incorporation of trace elements into pyrite during diagenesis of black shales, Yorkshire, England. Econ. Geol. 75 (5), 684–699.
- Raiswell, R., Canfield, D.E., Berner, R.A., 1994. A comparison of iron extraction methods for the determination of degree of pyritisation and the recognition of iron-limited pyrite formation. Chem. Geol. 111 (1–4), 101–110.
- Richardson, J.B., Aguirre, A.A., Buss, H.L., Toby O'Geen, A., Gu, X., Rempe, D.M., Richter, D.D.B., 2018. Mercury Sourcing and Sequestration in Weathering Profiles at Six Critical Zone Observatories. Global Biogeochem. Cycles 32 (10), 1542–1555.
- Román-Sánchez, A., Vanwalleghem, T., Peña, A., Laguna, A., Giráldez, J.V., 2018. Controls on soil carbon storage from topography and vegetation in a rocky, semi-arid landscapes. Geoderma 311, 159–166.

- Schroeder, P. (2018). Clays in the Critical Zone. Cambridge: Cambridge University Press. doi:10.1017/9781316480083.
- Shiller, A.M., Frilot, D.M., 1996. The geochemistry of gallium relative to aluminum in Californian streams. Geochim. Cosmochim. Acta 60 (8), 1323–1328.
- Sobecki, T.M., Karathanasis, A.D., 1992. Soils on hillslopes in acid gray and black shales. Soil Sci. Soc. Am. J. 56 (4), 1218–1226.
- United States Energy Information Administration and Kuuskraa, V., 2011. World shale gas resources: an initial assessment of 14 regions outside the United States. US Department of Energy.
- Vine, J.D., Tourtelot, E.B., 1970. Geochemistry of black shale deposits; a summary report. Econ. Geol. 65 (3), 253–272.
- White, T.S. and Dere, A.L.D., 2014. Rates of tree throw in Appalachian shale landscapes. AGUFM, 2014, pp.EP13E-06.
- Yesavage, T., Fantle, M.S., Vervoort, J., Mathur, R., Jin, L., Liermann, L.J., Brantley, S.L., 2012. Fe cycling in the Shale Hills Critical Zone Observatory, Pennsylvania: an analysis of biogeochemical weathering and Fe isotope fractionation. Geochim. Cosmochim. Acta 99, 18–38.
- Zhu, W., Young, L.Y., Yee, N., Serfes, M., Rhine, E.D., Reinfelder, J.R., 2008. Sulfide-driven arsenic mobilization from arsenopyrite and black shale pyrite. Geochim. Cosmochim. Acta 72 (21), 5243–5250.